energy&fuels

Article

pubs.acs.org/EF

Fe−Ni−MCM-41 Catalysts for Hydrogen-Rich Syngas Production from Waste Plastics by Pyrolysis−Catalytic Steam Reforming

Yeshui Zhang,[†] Jun Huang,*[,‡] and Paul T. Williams*[,†]

[†]School of Chemical and Process Engineering, University of Leeds, Leeds LS2 9JT, United Kingdom

[‡]Laboratory for Catalysis Engineering, School of Chemical and Biomolecular Engineering, The University of Sydney, Sydney, New South Wales 2006, Australia

ABSTRACT: A two-stage pyrolysis−catalytic steam reforming process was used with mesoporous MCM-41 supported iron and nickel bimetallic catalysts for hydrogen-rich syngas production from a simulated mixture of waste plastics. Different Fe/Ni weight ratios (00:20, 05:15, 10:10, 05:15, and 20:00) have been investigated to determine the influence on hydrogen production. The results showed that the presence of Fe and Ni together produced a synergistic enhancement of the total gas yield and hydrogen and carbon monoxide production. For example, the (10:10) Fe−Ni−MCM-41 catalyst produced the highest gas yield of 95 wt %, the highest H_2 production of 46.1 mmol H_2 $g^{-1}_{plastic}$, and the highest CO production at 31.8 mm $g^{-1}_{plastic}$. The (10:10) Fe−Ni−MCM-41 catalyst produced a volumetric hydrogen concentration of 46.7 vol %, and carbon monoxide was 32.2 vol %. The (10:10) Fe−Ni−MCM-41 catalyst also showed the lowest carbon deposition on the catalyst. The carbon deposits were mainly of the amorphous encapsulating type for the iron catalyst, but when nickel was present, the carbon deposits were mainly filamentous. The carbon deposits were also analyzed by transmission electron microscopy with energy-dispersive X-ray spectroscopy elemental mapping and showed that the iron/nickel metal particles were involved in the formation of the filamentous carbons, which were found to be both solid and hollow filaments.

1. INTRODUCTION

The demand for plastics in Europe is 49 million tonnes (Mt) per year, which are mainly used as packaging material (39.9%), in the building and construction industry (19.7%), in the automotive industry (8.9%), in electrical and electronic goods (5.8%), and in the agricultural industry (3.3%).[1] In addition, 22.4% of plastic is used in various other applications, such as consumer goods, furniture, sports equipment, etc. The most commonly used plastics in Europe are polypropylene (PP, ∼8.5 Mt $year^{-1}$ usage), low-density polyethylene (LDPE, 8.0 Mt $year^{-1}$ usage), high-density polyethylene (HDPE, 5.5 Mt $year^{-1}$ usage), polyvinyl chloride (PVC, 4.9 Mt $year^{-1}$ usage), polyurethane (PU, 3.3 Mt $year^{-1}$ usage), polyethylene terephthalate (PET, 3.0 Mt $year^{-1}$ usage), and polystyrene (PS, 1.9 Mt $year^{-1}$ usage). The plastic material will eventually end up as waste, and each year approximately 26 Mt of waste plastics are generated across Europe, the majority of which is recycled or used in energy recovery processes but more than 30% is landfilled, representing a waste of resource.[1] Consequently, novel technologies for the utilization of the waste plastics are under investigation, including the production of higher value products, such as hydrogen, as an energy carrier for the predicted future hydrogen economy.[2]

Around 96% of hydrogen is currently produced from fossil fuels by processes such as natural gas reforming (48%), oil/naphtha reforming (30%), and coal gasification (18%). Using waste plastics to generate hydrogen would represent a novel route to recycle plastics while also acting as an alternative feedstock.[3] Many researchers have studied the thermal decomposition of plastics with the aim of producing hydrogen.[4−8] Two-stage processes for the production of waste plastics have been employed by several researchers, whereby the waste plastic is first pyrolyzed in a first-stage pyrolysis process to produce a range of pyrolysis gases, which are then passed to a second-stage catalytic reactor, where catalytic steam reforming takes place to generate hydrogen.[3−8] The process is similar to the catalytic steam reforming of natural gas.[3]

Catalysts play a key role in maximizing hydrogen production from the pyrolysis−catalytic steam reforming of waste plastics. Nickel-based catalysts are the most common catalyst for the commercial production of hydrogen from natural gas catalytic steam reforming because of their high thermal stability and selectivity toward hydrogen production and, hence, have been applied for the pyrolysis−catalytic steam reforming of waste plastics.[3,4,7−9] Other transition metals have been investigated for the catalytic steam reforming of various feedstocks. For example, Hu and Lu[10] investigated the catalytic steam reforming of acetic acid over Ni, Fe, Co, and Cu alumina catalysts for the production of hydrogen. Ni and Co alumina catalysts showed good catalytic activity for the production of hydrogen via the catalytic steam reforming reaction, whereas Fe alumina promoted the water-gas shift reaction for H_2 production. Aupretre et al.[11] also investigated various transition metals, including nickel, iron, zinc, and copper, as well as noble metals on an alumina support for the production of H_2 via the steam reforming of bioethanol. They also confirmed the higher catalytic activity for Ni alumina for the steam reforming reaction and the lower activity of Fe, Zn, and Cu alumina for steam reforming but higher activity for the water-gas shift reaction. Acomb et al.[12,13] used a two-stage pyrolysis−catalytic

Received: May 11, 2017
Revised: June 23, 2017
Published: July 11, 2017

DOI: 10.1021/acs.energyfuels.7b01368
Energy Fuels 2017, 31, 8497−8504

Table 1. Ultimate Analysis of the Plastic Material

sample	N (wt %)	C (wt %)	H (wt %)	O (wt %)	S (wt %)
high-density polyethylene (HDPE)	0.94	80.58	18.48	nd[a]	nd[a]
low-density polyethylene (LDPE)	0.94	81.01	18.06	nd[a]	nd[a]
polypropylene (PP)	0.95	80.58	10.42	10.42	nd[a]
polystyrene (PS)	0.86	86.19	12.43	12.43	nd[a]
polyethylene terephthalate (PET)	0.57	61.0	11.30	27.13	nd[a]

[a]nd = not detected.

steam reforming process using Ni, Fe, Co, and Cu alumina catalysts for hydrogen production from low-density polyethylene. The Fe alumina catalyst gave the highest production of hydrogen from polyethylene compared to the other catalysts.

The use of different catalyst supports also has an effect on the performance of a catalyst through the interaction of the active metal with the support, surface area and porosity of the support material, etc. Miyazawa et al.[14] investigated the performance of nickel catalysts on various supports for the steam reforming of biomass pyrolysis tars.[14] Ni−Al_2O_3, Ni−ZrO_2, Ni−TiO_2, Ni−CeO_2, and Ni−Ni−MgO catalysts were examined. The Ni−Al_2O_3 catalyst was found to be the most active, and the Ni−MgO catalyst was found to be the least active, in relation to hydrogen production. It was suggested that the type of support used influenced the nickel metal particle size, which was a key to catalyst activity. Inaba et al.[15] investigated Ni−SiO_2, Ni−ZrO_2, Ni−CeO_2, and a series of Ni zeolites for use as catalysts for hydrogen production from the gasification of cellulose. The production of hydrogen followed the order: Ni-SiO_2 > Ni−ZrO_2 > Ni−CeO_2. The production of hydrogen using the Ni zeolites was dependent upon the type of zeolite used.

MCM-41 is a mesoporous material that has a high surface area that can be up to 1000 $m^2\ g^{-1}$ and pore diameters of ∼2−10 nm with a flexible structure of the amorphous silica walls.[16] It has been used as the catalyst for hydrogen production; for example, Wu et al.[16] investigated Ni on a MCM-41 support for H_2 production from biomass, and Zhao et al.[17] compared Ni−Al_2O_3 and Ni−MCM-41 supports for hydrogen production from cellulose. Zhao et al.[17] reported that the highly ordered mesoporous structure of the MCM-41 support improved the dispersion of the active nickel particles and subsequently increased the interaction between the nickel sites and gaseous products. However, there are few reports investigating the production of H_2 from waste plastics using Ni−MCM-41. In addition, Aupretre et al.[11] have reported that Fe-based catalysts are effective for the production of hydrogen from carbon monoxide via the water-gas shift reaction. Pyrolysis of mixed plastics containing polyethylene terephthalate has been reported to produce carbon monoxide in addition to a range of hydrocarbon gases.[18] Therefore, combining Ni and Fe on the MCM-41 support may enhance both the steam reforming reaction and the water-gas shift reaction in a combined pyrolysis−catalytic process in the presence of steam. Nickel- and iron-based catalysts with different crystal sizes have been investigated in thermochemical conversion processes to produce hydrogen in our previous research.[19] The results showed that the Fe-based catalyst produced an increased amount of hydrogen compared to the Ni-based catalyst. In addition, the Fe-based catalyst also produced a higher amount of carbon production as a result of the relatively high carbon solubility of iron particles.

In this paper, iron and nickel bimetallic catalysts have been investigated with different Fe/Ni ratios using the MCM-41 support for the production of hydrogen from simulated mixed waste plastics (SMWPs) using a two-stage pyrolysis−catalytic steam reforming process.

2. MATERIALS AND METHODS

2.1. Materials. The SMWP used in the experiments was a mixture of pure and waste plastic pellets with 2−3 mm diameters, and the SMWP sample contained 42 wt % LDPE, 20 wt % HDPE, 16 wt % PS, 12 wt % PET, and 10 wt % PP. HDPE, PP, and PS were purchased from Regain Polymers, Ltd., Castleford, U.K., a U.K. plastic recycling company. LDPE was purchased from Sigma-Aldrich, Ltd., U.K., and PET was purchased from Goodfellow, Ltd., U.K. The mixture of plastics was based on a typical composition of residual waste plastics found in municipal solid waste as reported by Delgado et al.[20] The ultimate analysis of each raw material was analyzed by a FLASH EA2000 CHNS analyzer; oxygen was calculated by difference; and the results are shown in Table 1. The nitrogen contents in all of the plastic samples were very low. Some of the real waste plastics, including PP and PS, contained significant amounts of oxygen, probably as a result of contamination with other plastic materials. PET, as expected, contained a large content of oxygen, at 27.13 wt %. No sulfur was found in any of the samples.

The Fe−Ni−MCM-41 catalysts with different Fe/Ni ratios were synthesized by an impregnation method.[12] The required calculated amounts of iron nitrate and nickel nitrate were dissolved in ethanol to form a solution. MCM-41 powder was synthesized according to the method reported by Cheng et al.,[21] added to the solution, and continuously stirred for 2 h until the mixture became a slurry. The slurry was dried overnight at 80 °C, and the solid was calcined in a muffle furnace heated at 1 °C min^{-1} ramp rate to a final temperature of 550 °C and held at that temperature for 4 h in the presence of static air. Fe−Ni−MCM-41 catalysts with Fe/Ni ratios of 00:20, 05:15, 10:10, 15:05, and 20:00 by weight percentage of metal were prepared. Adding transition metals in increasing concentrations has been shown to increase metal dispersion and reduce the reduction temperature.[22] The catalyst metals were not reduced from their oxidized state after preparation, but reduction occurred by produced H_2 and CO during the process of pyrolysis reforming of the waste plastics.[23] Yung et al.[24] investigated the influence of catalyst pretreatment via catalyst reduction with hydrogen and non-reduction using Ni/ZSM-5 catalysts for the upgrading of biomass pyrolysis gases. They found that, while there was some initial catalyst activity differences between the non-reduced NiO/ZSM-5 catalyst and the pre-reduced Ni/ZSM-5 catalysts, the activity of the catalysts converged after increasing time on stream. The results suggested that *in situ* reduction of NiO occurs within the process by the reducing gases, such as H_2 and CO, produced from biomass pyrolysis. Their conclusion was also supported by characterization of the catalysts before and after reaction, including temperature-programmed reduction and X-ray diffraction (XRD) studies, confirming *in situ* catalyst reduction by the pyrolysis gases.

2.2. Experimental System. The pyrolysis−catalytic steam reforming of SMWP experiments were carried out in a two-stage fixed-bed reactor. The first stage consisted of pyrolysis of the waste plastic mixture, and the second stage consisted of catalytic steam reforming of the evolved pyrolysis gases over the Fe−Ni−MCM-41 catalyst. An additional water-gas shift reaction may also occur with evolved carbon monoxide derived from the waste plastics. Figure 1 shows a schematic diagram of the reactor system. The reactors were

DOI: 10.1021/acs.energyfuels.7b01368
Energy Fuels 2017, 31, 8497−8504

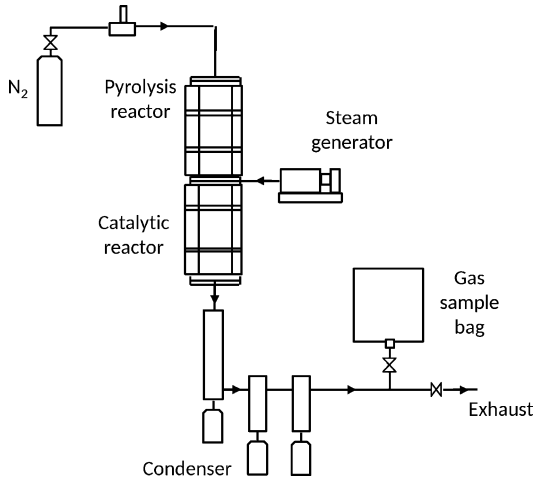

Figure 1. Schematic diagram of the two-stage fixed-bed pyrolysis−catalytic reforming reactor system.

made of stainless steel and were externally heated by temperature-controlled and monitored electric furnaces. The carrier gas was nitrogen and was introduced with a flow rate at 80 mL min^{-1}. The SMWP sample was placed in the pyrolysis reactor and pyrolyzed at 500 °C, and the Fe−Ni−MCM-41 catalyst was placed in the middle of the catalyst reforming reactor, where steam reforming occurred at 800 °C. A sample/catalyst ratio of 4:1 was used throughout this research. Steam was introduced into the catalytic reforming reactor process by controlling the water injection rate at 2 mL h^{-1}. Condensable products were collected in a water- and dry-ice-cooled triple condenser system, and non-condensable gases were collected in a Tedlar gas sample bag. The experimental procedure was preheating the catalytic reactor to 800 °C, followed by pyrolysis of the mixed waste plastics via heating from room temperature to 500 °C at a heating rate of 40 °C min^{-1}.

2.3. Analytical Methods. The gaseous products collected in the gas sample bag were analyzed directly after each experiment by two separate Varian 3380 gas chromatographs (GCs). The Varian GC used for permanent gas, including H_2, CO, O_2, and N_2, was fitted with a 2 m long, 2 mm diameter, 60−80 mm mesh molecular sieve column, a thermal conductivity detector, and argon carrier gas. CO_2 was also analyzed with this GC but via a separate GC HayeSep column, which was 2 m long, 2 mm diameter, with 80−100 mm mesh packing, with a separate thermal conductivity detector and argon carrier gas. The Varian GC used for hydrocarbon analysis from C_1−C_4 was fitted with an 80−100 mm mesh HayeSep column and a flame ionization detector with nitrogen as the carrier gas. The mass of gas was calculated from the determination of the gas volume percentage, the known quantity of nitrogen carrier gas and flow rate, the number of moles for each gas, and the molecular weights of all individual gases.

The morphology of the freshly prepared Fe−Ni−MCM-41 catalysts was examined using Hitachi SU8230 scanning electron microscopy (SEM). XRD analysis of the prepared and used catalysts was carried out on a Shimadzu 6000, which was used to identify the mineral phase composition of the catalysts with different Fe/Ni ratios. The Brunauer−Emmett−Teller (BET) surface areas of the fresh Fe−Ni−MCM-41 catalysts were determined by N_2 adsorption and desorption isotherms on a Autosorb IQ-C system and recorded at 77 K.

Deposited carbon on the surface of the catalysts after reaction was analyzed through temperature-programmed oxidation (TPO) using a Shimadzu thermogravimetric analyzer (TGA). A sample of the reacted catalyst was placed in the sample crucible of the TGA and heated to a temperature of 800 °C at a ramp rate of 15 °C min^{-1} in an air flow rate of 50 mL min^{-1}. Comparing the different oxidation characteristics of the reacted catalysts provides an indication of the different types of carbon deposited on the catalyst. The deposited carbons were also analyzed by Hitachi SU8230 SEM and also Tecnai TF20 transmission electron microscopy (TEM) fitted with an energy-dispersive X-ray spectroscopy (EDXS) system. The TEM−EDXS analysis allowed for the bimetallic interaction features of the reacted catalysts to be determined and elemental mapping of C, Fe, and Ni.

3. RESULTS AND DISCUSSION

3.1. Characterization of Fresh Catalysts. The properties of the fresh catalysts were determined to characterize the effects of iron addition into the nickel-based MCM-41-supported catalysts. Figure 2 shows the XRD spectra of the fresh catalysts.

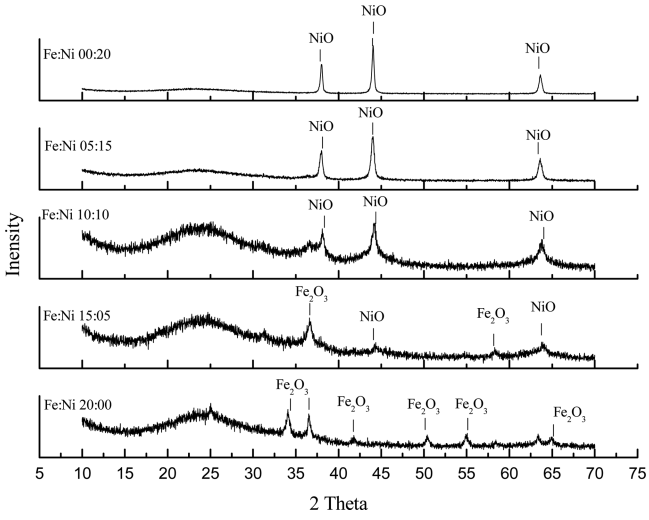

Figure 2. XRD analysis of fresh Fe−Ni−MCM-41 catalysts with different Fe/Ni ratios (00:20, 05:15, 10:10, 15:05, and 20:00).

As would be expected, the NiO phase was only observed for the fresh (00:20) Fe−Ni−MCM-41 catalyst, i.e., where no Fe was present, and the Fe_2O_3 phase was only observed for the (20:00) Fe−Ni−MCM-41 catalyst, i.e., where no Ni was present. However, when the bimetallic catalysts were analyzed, both NiO and Fe_2O_3 phases were observed for the fresh (05:15, 10:10, and 15:05) Fe−Ni−MCM-41 catalysts. In Figure 2, it can be seen that the signal intensity of the NiO phases decreased and the intensity of the Fe_2O_3 phases increased corresponding to the Fe/Ni ratio. The catalyst with only Fe loading showed that the presence of more Fe_2O_3 phases was observed in the XRD spectra. Figure 2 shows that the metals in the Fe−Ni−MCM41 catalysts were oxides, which will become reduced to the Ni and Fe metal by the reducing gases produced from the pyrolysis−catalytic reforming process, such as H_2 and CO.[23] The broad signal between 20° and 30° shown in Figure 2 is caused by the amorphous silica structure of MCM-41.

The surface area, total pore volumes, and average pore radius were determined by N_2 adsorption and desorption isotherms. Table 2 shows that the catalysts all had a surface area of ∼800 m^2 g^{-1}. There appeared to be no significant effects of the

Table 2. BET Surface Area, Pore Volume, and Average Pore Radius of Fe−Ni−MCM-41 Catalysts with Different Fe/Ni Ratios (00:20, 05:15, 10:10, 15:05, and 20:00)

Fe/Ni (wt %)	surface area (m^2 g^{-1})	total pore volume (cm^3 g^{-1})	average pore radius (nm)
00:20	826	6.42	1.55
05:15	777	6.01	1.55
10:10	802	6.31	1.57
15:05	781	6.28	1.61
20:00	800	6.29	1.57

DOI: 10.1021/acs.energyfuels.7b01368
Energy Fuels 2017, 31, 8497−8504

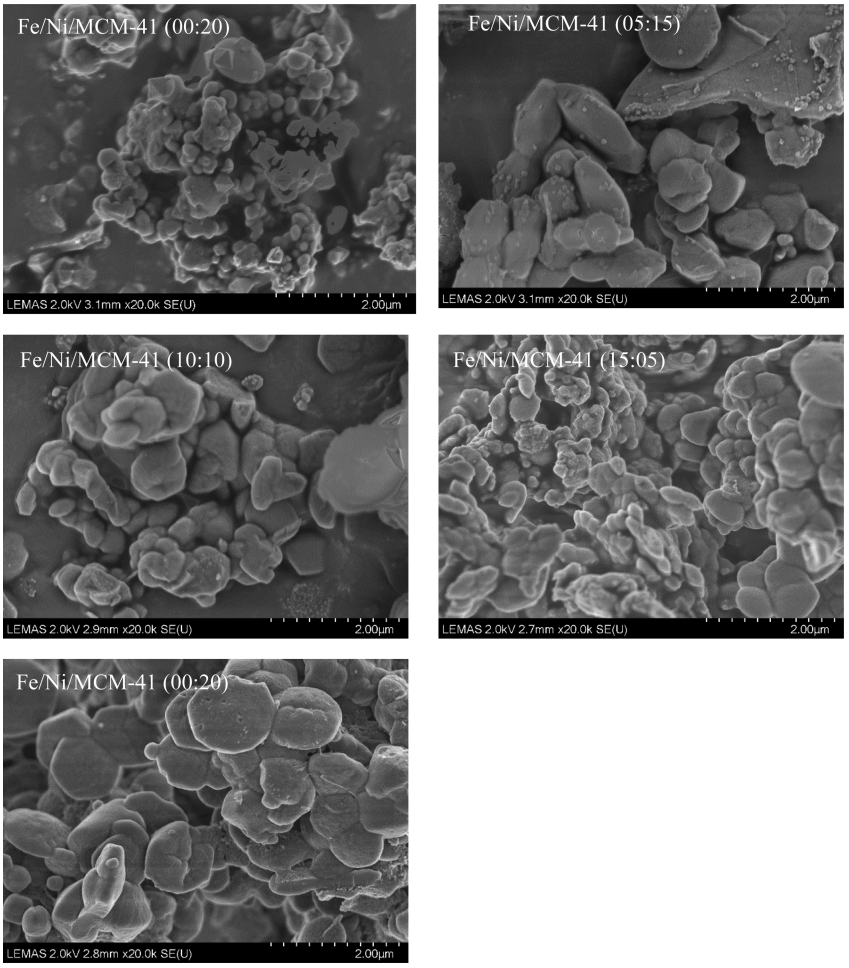

Figure 3. SEM fresh Fe−Ni−MCM-41 catalysts with different Fe/Ni ratios (00:20, 05:15, 10:10, 15:05, and 20:00).

amount of iron addition to the catalyst in terms of the surface area, pore volume, or pore radius of the catalysts. This could because the pore blockage caused by the metal iron and nickel oxides was at a similar level because the total metal loadings for each Fe/Ni ratio were maintained at 20 wt % for each catalyst. The morphology of the fresh Fe−Ni−MCM-41 catalysts with different Fe/Ni ratios was determined by SEM, and representative micrographs are shown in Figure 3. The fresh catalyst particles exhibited a fairly uniform particle size of between 0.5 and 1 μm.

3.2. Effect of the Fe/Ni Ratio on Gaseous Products. The MCM-41-supported catalysts with different Fe/Ni ratios were used in the pyrolysis−catalytic steam reforming process with the SMWPs in terms of determining the influence of the Fe/Ni ratio on hydrogen production. Figure 4 shows the XRD spectra for the used Fe−Ni−MCM-41 catalysts after the pyrolysis−catalytic steam reforming process of the waste plastics mixture. The results confirm that the catalysts were reduced from the metal oxides to the elemental metal within the initial stages of the process.[23] The results are shown in terms of the product yield and volumetric gas composition in Table 3. The gas yield in Table 3 is expressed in terms of the mass of plastic only, which, since steam (water) was injected, increases to over 100 wt % because some gas yield will also come from the reactions of the injected steam. In addition, the gas yield is also expressed as the yield in relation to the mass of plastics and reacted water. The mass closure for all of the

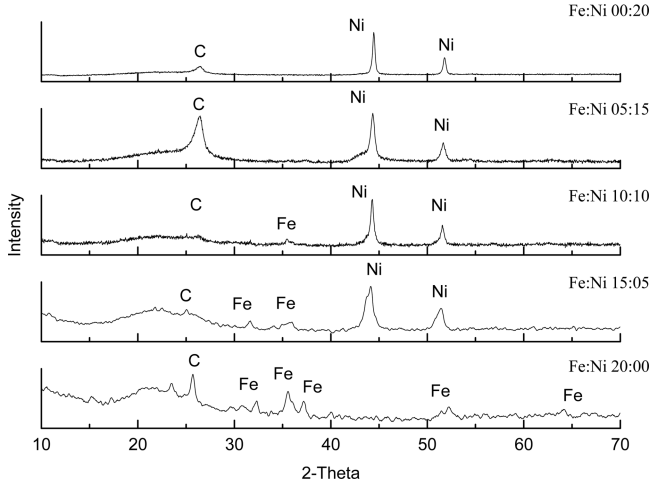

Figure 4. XRD analysis of the used Fe−Ni−MCM-41 catalysts from the pyrolysis−catalytic reforming of simulated mixed waste plastics with different Fe/Ni ratios (00:20, 05:15, 10:10, 15:05, and 20:00).

experiments was between 94 and 99 wt % when all reactants were taken into account. Table 3 shows that the gas yield in relation to the mass of plastics and reacted water for the nickel-only (00:20) Fe−Ni−MCM-41 catalyst was 84.9 wt %, and for the iron-only (20:00) Fe−Ni−MCM-41 catalyst, the gas yield was 73.5 wt %. In terms of hydrogen, the production was 30.5 and 18.1 mmol $g^{-1}_{plastic}$ for the Ni-only (00:20) Fe−Ni−MCM-

DOI: 10.1021/acs.energyfuels.7b01368
Energy Fuels 2017, 31, 8497−8504

Table 3. Product Yields and Gas Concentrations from Pyrolysis−Catalytic Reforming of SMWPs with Fe−Ni−MCM-41 Catalysts with Different Fe/Ni Ratios (00:20, 05:15, 10:10, 15:05, and 20:00)

	Fe/Ni ratio				
	00:20	05:15	10:10	15:05	20:00
gas yield in relation to mass of plastics (wt %)	111.9	101.2	155.9	122.2	89.1
carbon deposition (wt %)	16.0	14.5	6.0	7.0	10.0
gas yield in relation to plastics + reacted water (wt %)	84.9	82.8	95.0	86.0	73.5
mass balance in relation to plastics + reacted water (%)	93.82	95.4	95.29	98.77	93.94
H_2 production (mmol $g^{-1}_{plastics}$)	30.5	29.9	46.1	30.9	18.1
CO production (mmol $g^{-1}_{plastics}$)	13.1	8.5	31.8	19.8	8.4
syngas (H_2 + CO) production (mmol $g^{-1}_{plastics}$)	43.6	38.4	77.9	50.7	26.5
gas concentration (vol %, N_2 exclusive)					
CO	19.3	13.2	32.2	27.6	17.3
H_2	45.0	46.5	46.7	43.1	37.2
CO_2	3.4	3.0	1.9	2.5	3.4
CH_4	8.9	10.1	6.2	7.3	12.5
C_2−C_4	22.9	25.4	12.9	17.7	29.7

41 and Fe-only (20:00) Fe−Ni−MCM-41 catalysts, respectively. Nickel is reported to be more dominant for hydrogen production compared to iron as a result of the higher catalytic activity of nickel-based catalysts.[25] The results are consistent with our previous research with waste tires as the feedstock, where a Ni/Al_2O_3 catalyst produced higher gas and hydrogen compared to a Fe/Al_2O_3 catalyst in a pyrolysis catalytic−gasification process.[26]

However, for the (10:10) Fe−Ni−MCM-41 catalyst, the gas yield (in relation to plastics and reacted water) was significantly higher than would be expected from a merely additive effect, with a gas yield of 95.0 wt %. In addition the (10:10) Fe−Ni−MCM-41 catalyst produced the highest hydrogen production at 46.1 mm $g^{-1}_{plastic}$ and the highest CO production at 31.8 mm $g^{-1}_{plastic}$. The syngas (H_2 + CO) production from the pyrolysis−catalytic steam reforming of the mixed plastics was enhanced with the introduction of the Fe/Ni catalyst, particularly with the (10:10) Fe−Ni−MCM-41 catalyst producing 77.8 $mmol_{gas}$ $g^{-1}_{plastic}$. The results suggest a synergistic effect of nickel and iron, which enhances the catalytic activity by increasing the metal dispersion and reduction temperature toward the total gas yield and hydrogen production.[27] Zhang et al.[27] reported that metal dispersion had been improved by the synergy of Ni−Co as bimetallic catalysts. Becerra et al.[28] found that the number of surface metal atoms was significantly increased and, consequently, increased catalytic activity for a Ru−Ni bimetallic catalyst for carbon dioxide reforming of methane. Rynkowski et al.[29] also reported that the Ni−Pt bimetallic catalysts promote the metal dispersion on the catalyst, which is one of the most important factors that affects the catalyst activity. It is also noteworthy that the lowest catalyst carbon deposition also occurred with the (10:10) Fe−Ni−MCM-41 catalyst at 6.0 wt %. At different Fe/Ni ratios, there was less of a synergistic effect, with the (05:15) Fe−Ni−MCM-41 catalyst producing a lower gas yield and hydrogen production. The (15:05) Fe−Ni−MCM-41 catalyst showed an improved gas yield at 86.0 wt % and higher hydrogen production at 30.9 mm $g^{-1}_{plastic}$, but yields were lower than the (10:10) Fe−Ni−MCM-41 catalyst.

The relative volumetric gas compositions are also shown in Table 3. The gas product consisted of mainly hydrogen, carbon monoxide, methane, and C_2−C_4 hydrocarbons, with lower concentrations of carbon dioxide. The highest CO yield (32.2 vol %) occurred with the (10:10) Fe−Ni−MCM-41 catalyst, which also produced the highest hydrogen yield (46.7 vol %) and the lowest CO_2 (1.9 vol %), CH_4 (6.2 vol %), and C_2−C_4 (12.9 vol %) yields. Hydrogen and carbon monoxide produced from the simulated mixture of waste plastics by pyrolysis−catalytic steam reforming are based on the following equations:[16]

$$C + H_2O \rightarrow CO + H_2 \quad (1)$$

$$CO + H_2O \rightarrow CO_2 + H_2 \quad (2)$$

$$CH_4 + H_2O \rightarrow CO + 3H_2 \quad (3)$$

$$C_nH_m + H_2O \rightarrow nCO + (m + 2)/2H_2 \quad (4)$$

The maximum yield of syngas (hydrogen and carbon monoxide) produced was 78.9 vol % with the (10:10) Fe−Ni−MCM-41 catalyst, which promotes the conversion of the hydrocarbons to produce more CO and H_2 based on eqs 1−4. CO may be involved in the water-gas shift reaction (eq 2), producing more hydrogen, catalyzed by the presence of Fe in the catalyst.[11]

3.3. Effect of the Fe/Ni Ratio on Catalyst Carbon Deposition. Carbon produced from the pyrolysis−catalytic steam reforming of the SMWP process can encapsulate the active metal sites of the catalyst that will result in catalyst deactivation.[30] The conversion efficiency of the plastics in the catalytic steam reforming process could consequently decrease by catalyst deactivation depending upon the amount of carbon deposited but also the type of carbon deposited.[30,31] Different types of carbon may form on the catalyst, including encapsulating carbons, which lead to catalyst deactivation, and/or filamentous-type carbons, which have a lesser deactivation effect on the catalyst.[30] Therefore, the properties of deposited carbon on the catalyst were determined by a series of analyses: TPO was used to identify the type of carbon deposition, and SEM and TEM were used to characterize the morphology of carbon deposition.

Table 3 shows that the Fe/Ni ratio influenced the amount of carbon deposited on the catalysts, with the lowest at the Fe/Ni ratio of 10:10 (6.0 wt %) and the highest with the Ni-only catalyst (Fe/Ni ratio of 00:20) at 16.0 wt % deposited carbon. This could be caused by the synergistic effect between iron and nickel metals, which improves the carbon formation resistance as a result of the strong metal−support interaction. TPO of the carbon deposits showed that, for the catalyst that contained some nickel (05:15, 10:10, 15:05, and 20:00), the oxidation of carbon occurred at temperatures of over 670 °C, which indicates that most carbon deposited was filamentous carbon.[30] However, for the Fe-only catalyst (20:00 Fe−Ni−MCM-41), the oxidation of carbon occurred at less than 550 °C, indicating that carbon deposited was mainly amorphous carbon. SEM analysis was also carried out, and Figure 5 shows the SEM micrographs for the Fe/Ni MCM-41 catalysts after pyrolysis−catalytic steam reforming of the waste plastics. The SEM images for the reacted (00:20, 05:15, 10:10, and 15:05) Fe−

DOI: 10.1021/acs.energyfuels.7b01368
Energy Fuels 2017, 31, 8497−8504

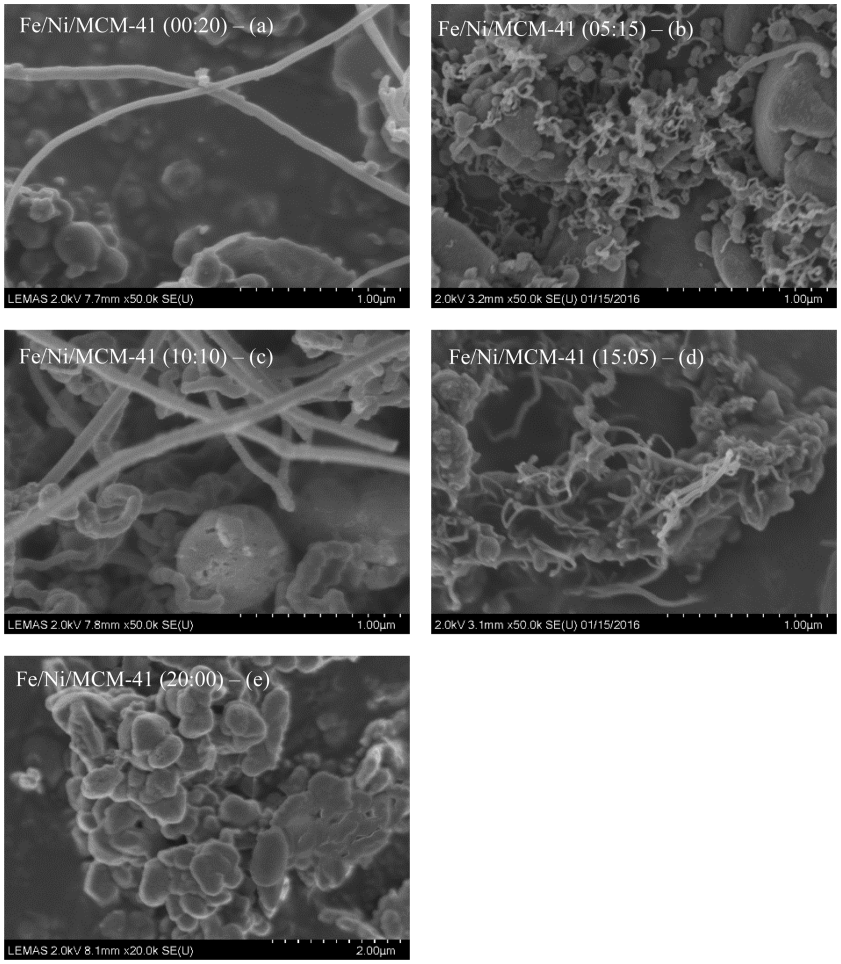

Figure 5. SEM images of the used catalysts from the pyrolysis−catalytic reforming of SMWPs with Fe−Ni−MCM-41 catalysts with different Fe/Ni ratios (00:20, 05:15, 10:10, 15:05, and 20:00).

Ni−MCM-41 catalysts show the presence of filamentous carbon. However, carbon produced with the Fe-only catalyst (20:00 Fe−Ni−MCM-4) showed few filamentous carbons, confirming that deposited carbon was mostly the amorphous type.

TEM−EDXS elemental mapping was carried out on the reacted bimetallic catalysts (containing both Fe and Ni) to determine the carbon, iron, and nickel locations on the catalyst. The specific TEM images for the different catalysts (05:15, 10:10, and 15:05 Fe−Ni−MCM-41) coupled with carbon, nickel, and iron mapping are shown in Figure 6. Figure 6a shows the TEM micrograph of the carbon deposits from the 05:15 Fe−Ni−MCM-41 catalyst from pyrolysis−catalytic steam reforming of the waste plastics. The carbon mapping coupled with the TEM images shows that carbon is distributed throughout all of the particles and filaments shown. However, Fe and Ni mapping of the same micrograph image shows that the darker particles shown in the TEM image are composed of both Fe and Ni. The TEM images of the metal particles shown in panels a−c of Figure 6 show that the particle size ranges from 5 nm to larger than 50 nm. The carbon deposits on all of the catalysts consisted of both solid carbon and also hollow carbon filaments; for example, panels b and c of Figure 6 for the used 10:10 and 15:05 Fe−Ni−MCM-41 catalysts show the presence of hollow carbon filaments. In addition, panels b and c of Figure 6 shows that the metal particle is located within the hollow filament or at the tip or base of the carbon filament.

There have been several reports suggesting the growth mechanism of the carbon filaments involving the interaction of the catalyst support and the metal.[30−36] It is suggested that the interaction of the hydrocarbons derived from pyrolysis saturates the bimetallic Fe and Ni particles with carbon species, such as metal carbides or reactive carbons.[31−34] The carbon species dissolve and diffuse into the bimetal particles and then precipitate to grow filaments away from the catalyst surface or grow between the metal and support to lift the metal particle with the filament formation.[35] Whether the carbon filaments grow from the metal particle on the surface or lift the metal particle away from the surface depends upon the strength of the metal−support interaction.[36]

The results have shown overall that a syngas (H_2 + CO) with enhanced concentrations of hydrogen can be produced from waste plastics using a two-stage pyrolysis−catalytic steam reforming process using Fe−Ni−MCM-41 catalysts. Manipulating the Fe/Ni ratio can significantly raise the production of hydrogen and carbon monoxide from the plastics, with the 10:10 Fe/Ni ratio producing the greatest effect. Fe and Ni in the catalyst produced a synergistic enhancement of both H_2 and CO compared to the Fe-only and Ni-only MCM-41 catalysts. For example, for the Fe-only catalyst, the H_2 production was 18.1 mm $g^{-1}_{plastic}$ and CO was 8.4 mm $g^{-1}_{plastic}$, and for the Ni-

DOI: 10.1021/acs.energyfuels.7b01368
Energy Fuels 2017, 31, 8497−8504

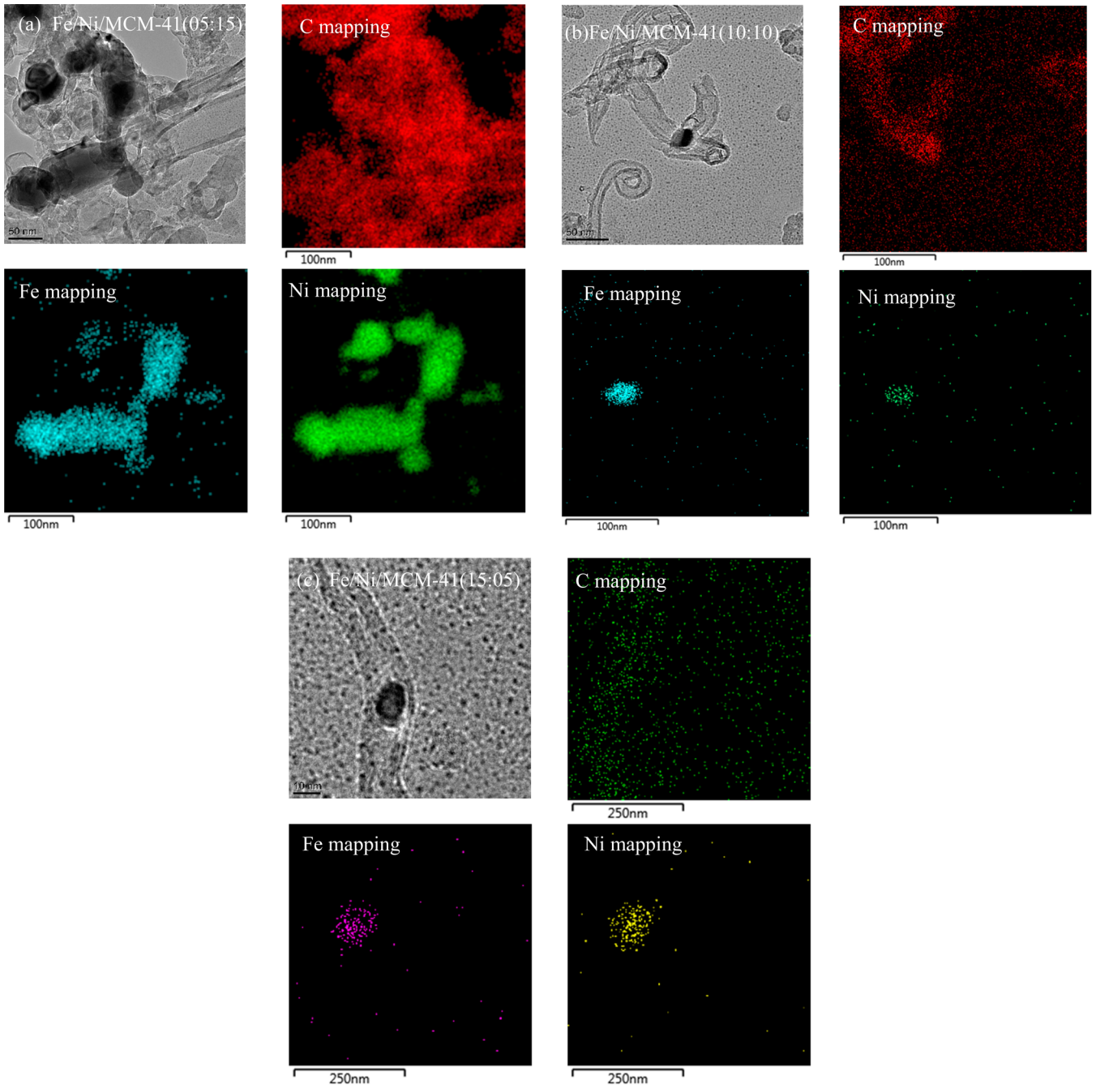

Figure 6. TEM−EDXS elemental mapping analysis of C, Fe, and Ni for reacted (05:15, 10:10, and 15:05) Fe−Ni−MCM-41 catalysts.

only catalyst, H_2 production was 30.5 mm $g^{-1}_{plastic}$ and CO was 13.1 mm $g^{-1}_{plastic}$. The calculated calorific value of the product gases was between 20.8 and 31.8 MJ m^{-3}, depending upon the Fe/Ni ratio, representing a useful product fuel gas. The highest calorific value of the product gas was for the Fe-only catalyst at 31.8 MJ m^{-3} as a result of the high content of C_1−C_4 gases produced.

4. CONCLUSION

Waste plastics have been processed using a two-stage pyrolysis−catalytic steam reforming process system to produce a hydrogen-enhanced syngas using various Fe/Ni ratios supported on MCM-41 catalysts. The iron and nickel bimetallic catalysts promoted the formation of hydrogen and carbon monoxide. A synergistic effect of iron and nickel was observed, particularly for the (10:10) Fe−Ni−MCM-41 catalyst, where the highest gas yield (95 wt %) and highest H_2 production (46.1 mmol $g^{-1}_{plastic}$) and CO production (31.8 mmol $g^{-1}_{plastic}$) were shown. The product syngas contained high volumetric concentrations of hydrogen and carbon monoxide with lower concentrations of C_1−C_4 hydrocarbons and CO_2. For example, the (10:10) Fe−Ni−MCM-41 catalyst produced a gas concentration of 46.7 vol % hydrogen, 32.2 vol % carbon monoxide, 6.2 vol % methane, 12.9 vol % C_1−C_4, and 1.9 vol % carbon dioxide. The process also resulted in significant deposition of carbon on the catalysts, with the (10:10) Fe−Ni−MCM-41 catalyst producing the lowest carbon deposition (6 wt %), the nickel-only (00:20) Fe−Ni−MCM-41 catalyst

DOI: 10.1021/acs.energyfuels.7b01368
Energy Fuels 2017, 31, 8497−8504

producing 16 wt % carbon deposition, and the iron-only (20:00) Fe−Ni−MCM-41 catalyst producing 10.0 wt % carbon deposition. TEM−EDXS elemental mapping of the used catalyst showed that the iron/nickel metal particles promoted the growth of the carbon deposits as carbon solid and hollow filaments.

AUTHOR INFORMATION

Corresponding Authors

*Telephone: +61-2-9351-7483. E-mail: jun.huang@sydney.edu.au.

*Telephone: +44-113432504. E-mail: p.t.williams@leeds.ac.uk.

ORCID

Paul T. Williams: 0000-0003-0401-9326

Notes

The authors declare no competing financial interest.

ACKNOWLEDGMENTS

This project has received funding from the European Union's Horizon 2020 Research and Innovation Programme under the Marie Sklodowski-Curie Grant Agreement 643322 (FLEXI-PYROCAT) and the Australian Research Council Discovery Projects (DP150103842).

REFERENCES

(1) PlasticsEurope. *Plastics—The Facts 2016*; PlasticsEurope: Brussels, Belgium, 2016.

(2) National Research Council and National Academy of Engineering. *The Hydrogen Economy: Opportunities, Costs, Barriers and R&D Needs*; National Academies Press: Washington, D.C., 2004.

(3) Czernik, S.; French, R. J. *Energy Fuels* **2006**, *20*, 754−758.

(4) He, M.; Xiao, B.; Hu, Z.; Liu, S.; Guo, X.; Luo, S. *Int. J. Hydrogen Energy* **2009**, *34*, 1342−1348.

(5) Park, Y.; Namioka, T.; Sakamoto, S.; Min, T.; Roh, S.; Yoshikawa, K. *Fuel Process. Technol.* **2010**, *91*, 951−957.

(6) Namioka, T.; Saito, A.; Inoue, Y.; Park, Y.; Min, T. J.; Roh, S. A.; Yoshikawa, K. *Appl. Energy* **2011**, *88*, 2019−2026.

(7) Wu, C.; Williams, P. T. *Appl. Catal., B* **2009**, *90*, 147−156.

(8) Wu, C.; Williams, P. T. *Fuel* **2010**, *89*, 3022−3032.

(9) Wu, C.; Williams, P. T. *Appl. Catal., B* **2009**, *87*, 152−161.

(10) Hu, X.; Lu, G. *Appl. Catal., B* **2010**, *99* (1−2), 289−297.

(11) Aupretre, F.; Descorme, C.; Duprez, D. *Catal. Commun.* **2002**, *3*, 263−267.

(12) Acomb, J.; Wu, C.; Williams, P. T. *Appl. Catal., B* **2016**, *180*, 497−510.

(13) Acomb, J.; Wu, C.; Williams, P. T. *J. Anal. Appl. Pyrolysis* **2015**, *113*, 231−238.

(14) Miyazawa, T.; Kimura, T.; Nishikawa, J.; Kado, S.; Kunimori, K.; Tomishige, K. *Catal. Today* **2006**, *115* (1−4), 254−262.

(15) Inaba, M.; Murata, K.; Saito, M.; Takahara, I. *Energy Fuels* **2006**, *20*, 432−438.

(16) Wu, C.; Dong, L.; Onwudili, J.; Williams, P. T.; Huang, J. *ACS Sustainable Chem. Eng.* **2013**, *1*, 1083−1091.

(17) Zhao, M.; Florin, N. H.; Harris, A. T. *Appl. Catal., B* **2009**, *92*, 185−193.

(18) Williams, P. T.; Williams, E. A. *Energy Fuels* **1999**, *13*, 188−196.

(19) Liu, X.; Zhang, Y.; Nahil, M. A.; Williams, P. T.; Wu, C. *J. Anal. Appl. Pyrolysis* **2017**, *125*, 32−39.

(20) Delgado, C.; Barruetabeña, L.; Salas, O. *Assessment of the Environmental Advantages and Drawbacks of Existing and Emerging Polymers Recovery Processes*; Wolf, O., Ed.; Joint Research Centre, European Commission: Luxembourg, Luxembourg, 2007; EUR 22939 EN, DOI: 10.2791/46661.

(21) Wu, C.; Wang, L.; Williams, P. T.; Shi, J.; Huang, J. *Appl. Catal., B* **2011**, *108−109*, 6−13.

(22) Mu, S.; Li, D.; Hou, B.; Jia, L.; Chen, J.; Sun, Y. *Energy Fuels* **2010**, *24* (7), 3715−3718.

(23) Gao, N.; Liu, S.; Han, Y.; Xing, C.; Li, A. *Int. J. Hydrogen Energy* **2015**, *40*, 7983−7990.

(24) Yung, M. M.; Starace, A. K.; Mukarakate, C.; Crow, A. M.; Leshnov, M. A.; Magrini, K. A. *Energy Fuels* **2016**, *30* (7), 5259−5268.

(25) Dong, L.; Wu, C.; Ling, H.; Shi, J.; Williams, P. T.; Huang, J. *Energy Fuels* **2017**, *31*, 2118−2127.

(26) Zhang, Y.; Wu, C.; Nahil, M. A.; Williams, P. T. *Energy Fuels* **2015**, *29* (5), 3328−3334.

(27) Zhang, J.; Wang, H.; Dalai, A. K. *J. Catal.* **2007**, *249* (2), 300−310.

(28) Becerra, A.; Iriarte, E.; Dimitrijewits, M.; Castro-Luna, A. *Bol. Soc. Chil. Quim.* **2002**, *47*, 385−392.

(29) Rynkowski, J. M.; Paryjczak, T.; Lenik, M.; Farbotko, M.; Góralski, J. *J. Chem. Soc., Faraday Trans.* **1995**, *91* (19), 3481−3484.

(30) Wu, C.; Williams, P. T. *Appl. Catal., B* **2010**, *96*, 198−207.

(31) Sutton, D.; Kelleher, B.; Ross, J. R. H. *Fuel Process. Technol.* **2001**, *73*, 155−173.

(32) Louis, B.; Vieira, R.; Carvalho, A.; Amadou, J.; Ledoux, M. J.; Pham-Huu, C. *Top. Catal.* **2007**, *45*, 75−80.

(33) Sacco, A.; Hacker, P.; Chang, T. N.; Chiang, A. T. S. *J. Catal.* **1984**, *85*, 224−236.

(34) Kock, A. J. H. M.; Detoks, P. K.; Bolleaard, E.; Klop, W.; Geus, J. W. *J. Catal.* **1985**, *96*, 468−480.

(35) Rostrup-Nielsen, J. R.; Trimm, D. L. *J. Catal.* **1977**, *48*, 155−165.

(36) Kumar, M. Carbon nanotube synthesis and growth mechanism. In *Carbon Nanotubes—Synthesis, Characterization, Applications*; Yellampalli, S., Ed.; InTech: Rijeka, Croatia, 2011; Chapter 8, DOI: 10.5772/19331.

DOI: 10.1021/acs.energyfuels.7b01368
Energy Fuels 2017, 31, 8497−8504